Integrated proteomic and metabolomic profiling reveals molecular signatures underlying invasiveness in non-functioning pituitary adenomas

JIANYAO MAO[1*], XI CHEN[1*], WENTAO ZHENG[1*], BOSEN LIU[1*], ZHANGYU LI[1], YUKUI LI[1], PING ZHONG[1], SIFANG CHEN[1], GUOWEI TAN[1], CHEN WANG[2] and JINLI SUN[3]

[1]Department of Neurosurgery, The First Affiliated Hospital of Xiamen University, School of Medicine, Xiamen University, Xiamen, Fujian 361003, P.R. China; [2]Department of Neurology, Xiamen Xianyue Hospital, Xianyue Hospital Affiliated with Xiamen Medical College, Fujian Psychiatric Center, Fujian Clinical Research Center for Mental Disorders, Xiamen, Fujian 361012, P.R. China; [3]Department of Reproduction, The First Affiliated Hospital of Xiamen University, School of Medicine, Xiamen University, Xiamen, Fujian 361003, P.R. China

Received August 13, 2025; Accepted February 9, 2026

DOI: 10.3892/ol.2026.15521

Abstract. Pituitary adenomas constitute 10 to 25% of intracranial tumors, rendering them one of the most prevalent types of brain tumors. While the majority of pituitary adenomas are benign, ~35% exhibit invasive behavior. Compared with their non-invasive counterparts, invasive pituitary adenomas are more challenging to manage, highlighting the need to elucidate their underlying pathogenesis. However, the molecular mechanisms driving the invasive behavior of these tumors remain incompletely understood. Thus, the present study employed an integrated proteomic and metabolomic approach to investigate the molecular features associated with tumor invasiveness in pituitary adenomas. The investigation was performed at the First Affiliated Hospital of Xiamen University (Xiamen, China). Fresh-frozen tumor specimens were collected from 16 patients diagnosed with clinically non-functioning pituitary adenomas. These samples were divided into two groups based on invasiveness: Invasive tumors (n=8; Knosp grade ≥2) and non-invasive tumors (n=8; Knosp grade <2). Using data-independent acquisition mass spectrometry (MS) in conjunction with liquid chromatography-MS/MS metabolomics analysis, differentially expressed proteins (DEPs) and differentially expressed metabolites (DEMs) were identified. Comparative analysis identified 614 DEPs, including 286 proteins that were upregulated and 328 that were downregulated in invasive tumors relative to non-invasive tumors. Additionally, 74 DEMs were found, comprising 42 increased and 32 decreased metabolites. Enrichment analysis of pathways revealed notable involvement of the cyclic adenosine monophosphate (cAMP) signaling cascade, pathways related to pathogenic *Escherichia coli* (*E. coli*) infection and the synaptic vesicle cycle. Integration of the proteomic and metabolomic data underscored consistent changes within these biological pathways. The present investigation represents a comprehensive effort to combine proteomic and metabolomic approaches to characterize the invasive phenotype of pituitary adenomas. The identification of enriched pathways associated with cAMP signaling, *E. coli* infection and synaptic vesicle cycling provides new mechanistic understanding and offers potential biomarkers or therapeutic targets for differentiating tumor aggressiveness.

Correspondence to: Dr Jinli Sun, Department of Reproduction, The First Affiliated Hospital of Xiamen University, School of Medicine, Xiamen University, 55 Zhenhai Road, Xiamen, Fujian 361003, P.R. China
E-mail: sunkinglily@xmu.edu.cn

*Contributed equally

Abbreviations: DEP, differentially expressed protein; DEM, differentially expressed metabolite; LC-MS/MS, liquid chromatography-tandem mass spectrometry

Key words: proteomics, metabolomics, pituitary adenoma, tumor invasion, cAMP signaling, *Escherichia coli* infection, synaptic vesicle cycle

Introduction

Pituitary adenomas represent one of the most frequently occurring intracranial tumors globally, constituting 10 to 15% of all primary brain neoplasms (1). These tumors originate from the adenohypophysis and can lead to severe clinical manifestations, including systemic complications of the cardiovascular and metabolic systems, as well as permanent visual deficits due to the compression of surrounding structures, such as the optic chiasm, by the tumor (mass effect). Although most pituitary adenomas are histologically non-cancerous and show a slow-growing clinical course, a certain group exhibits invasive characteristics, marked by the penetration into adjacent tissues such as the cavernous sinus, dura mater or sphenoid sinus (2). These invasive pituitary adenomas (IPAs) are often associated with treatment resistance, increased recurrence rates and worse clinical outcomes, despite lacking malignant histopathological

features (3-5). Growing evidence suggests that metabolic reprogramming and mitochondrial dysfunction serve pivotal roles in the acquisition of aggressive phenotypes in various tumors. In the context of pituitary adenomas, alterations in energy metabolism and mitochondrial respiratory chains have been implicated in promoting tumor cell survival and invasion. However, a systematic understanding of the molecular landscape specifically associated with these metabolic shifts remains limited.

Recent advances in omics technologies, including proteomics and metabolomics, have provided powerful tools to explore tumor biology at the systems level. Proteomic and metabolomic approaches offer complementary insights into protein expression dynamics and metabolic alterations, critical for elucidating tumor biology. While proteomics provides a snapshot of the functional effectors of the cell, metabolomics offers a downstream functional readout of the cellular physiological state. Integrated analysis of these datasets can reveal the molecular mechanisms underlying tumor progression and metabolic reprogramming (6,7). Such high-throughput screening is essential for identifying key biomarkers that might be overlooked by traditional single-molecule studies.

In the present study, quantitative profiling of proteins and metabolites was performed in human pituitary adenoma tissues, comparing invasive and non-invasive subtypes. Specifically, the study focused on non-functioning pituitary adenomas to minimize the confounding effects of excessive hormone secretion on the metabolic profile. By identifying markedly dysregulated molecular features and assessing their enrichment in relevant biological pathways, particularly those involving mitochondrial function and energy pathways, the present study aimed to delineate the molecular and metabolic determinants of tumor invasion. The findings indicate that coordinated molecular perturbations contribute to the aggressive behavior of invasive pituitary adenomas, providing novel insights into potential therapeutic targets and supporting future mechanistic investigations into the metabolic drivers of tumor progression.

Materials and methods

Patients. This study was designed as a prospective recruitment of patients undergoing surgical resection for pituitary adenomas. A comparative analysis of 2 patient cohorts was performed to elucidate the proteomic and metabolic determinants associated with varying degrees of pituitary tumor aggressiveness. Tumors assigned a Knosp grade (8) of ≥2 were classified as invasive, whereas those <2 were categorized as non-invasive. The inclusion criteria for the pituitary adenoma samples were as follows: i) Patients had not received any prior medical, radiological, or surgical treatment before the study; ii) a preoperative clinical diagnosis of pituitary adenoma; iii) availability of tumor tissue samples resected during surgery; and iv) postoperative pathological confirmation of the pituitary adenoma diagnosis. The exclusion criteria included: i) Patients who had undergone any prior medical, radiological or surgical treatment; and ii) cases where the postoperative pathological diagnosis excluded pituitary adenoma. Additionally, patients who failed to complete the planned surgery or those from whom tumor tissue samples could not be retained were excluded from the final analysis. Patient tumor samples were collected between September 2023 and May 2024 at The First Affiliated Hospital of Xiamen University (Xiamen, China). Statistical analyses were performed using appropriate parametric or non-parametric tests depending on data type and distribution. Continuous variables were compared using unpaired Student's t-test for two-group comparisons or one-way ANOVA followed by Tukey's post hoc test for multiple-group comparisons. Categorical variables, including sex, were analyzed using Fisher's exact test. A P-value <0.05 was considered to indicate a statistically significant difference.

Proteomic analysis and protein quantification. Freshly resected pituitary adenoma tissues were taken from liquid nitrogen storage and quickly transferred onto ice. Samples were reconstituted in a lysis buffer containing 8 M urea and 1% SDS, supplemented with a 1% protease inhibitor cocktail to prevent enzymatic degradation. Homogenization was performed using a high-throughput tissue grinder for three consecutive cycles of 180 sec. This procedure was followed by cryogenic, non-contact sonication for 30 min. The resulting lysates were centrifuged at 16,000 x g for 30 min at 8˚C. Protein concentrations in the supernatants were quantified using the bicinchoninic acid (BCA) assay, according to the manufacturer's protocol (BCA Protein Assay Kit; Thermo Fisher Scientific, Inc.). Subsequently, SDS-PAGE was employed to separate the extracted proteins using a 12% separation gel, with 20 μg of protein loaded per lane.

Protein digestion. A total of 100 μg protein was dissolved in triethylammonium bicarbonate (TEAB) buffer to a final concentration of 100 mM. Reduction was performed using 10 mM tris(2-carboxyethyl)phosphine at 37˚C for 1 h to disrupt disulfide bonds. Alkylation was then performed with 40 mM iodoacetamide at room temperature for min in the dark to preserve the reactivity of the alkylating agent. Following these treatments, the samples were centrifuged at 10,000 x g for 20 min at 4˚C to eliminate soluble contaminants, yielding a protein pellet. The pellet was resuspended in 100 μl TEAB buffer, maintaining the buffer concentration at 100 mM. Proteins were digested by adding trypsin at an enzyme-to-substrate ratio of 1:50 and incubating overnight at 37˚C to produce peptides for subsequent analysis.

Peptide desalting and quantification. Following trypsin-mediated proteolysis, peptides were dried to completeness using a vacuum concentrator. The resulting desiccated peptides were reconstituted in 0.1% trifluoroacetic acid and purified via desalting with hydrophilic-lipophilic balanced cartridges. After purification, the samples were once again vacuum-dried. Peptide concentrations were quantified based on ultraviolet absorbance using a NanoDrop One spectrophotometer (Thermo Fisher Scientific, Inc.), following the manufacturer's standard operating protocol.

Data-independent acquisition (DIA) mass detection. Quantified peptide concentrations were subjected to analytical processing using the Vanquish Neo liquid chromatography (LC) system and the Compass HyStar interface developed by Bruker Corporation. All analyses were performed by Shanghai

Majorbio Bio-Pharm Technology Co., Ltd. Mass spectrometry was conducted in positive ionization mode. Chromatographic separation was performed on a custom-packed analytical column (15 cm x 100 μm) filled with 1.7 μm particles designed to enhance peptide resolution. For the electrospray source, the nitrogen gas temperature was set at 180˚C, the nebulizer pressure was maintained at 2.0 bar and the dry gas flow rate was 8.0 l/min. The separation process employed a binary solvent system consisting of solvent A (2% acetonitrile and 0.1% formic acid in water) and solvent B (80% acetonitrile and 0.1% formic acid in water), maintained over an 8-min linear gradient. Subsequent peptide detection was performed using a timsTOF HT mass spectrometer operated in DIA mode. Mass spectra were acquired within the m/z ranges of 70-1,050 for MS1 and 150-2,000 for MS2, enabling in-depth characterization of the peptide profiles. Mass spectrometry (MS) acquisition was performed in dia-PASEF mode. Each acquisition cycle consisted of multiple isolation windows, with each window defined by a specific m/z range and its corresponding ion mobility interval. The DIA isolation windows included the Mass Begin and Mass End boundaries for each m/z segment, the associated $1/K_0$ mobility ranges (Begin/End) and the collision energy (CE), which was dynamically ramped according to the ion mobility interval. The total cycle time for one full dia-PASEF acquisition cycle was 0.73 sec, and all remaining timsTOF instrument parameters followed manufacturer-recommended settings for quantitative proteomics.

Protein identification. The raw files from DIA were evaluated utilizing Spectronaut software (version 19; Biognosys AG). In the course of conducting the database search, parameters were set to restrict peptide lengths within the range of 7 to 52 amino acids. For enzymatic cleavage, trypsin/P was designated, permitting up to two missed cleavage sites. Fixed modifications included carbamidomethylation of cysteine residues, while methionine oxidation and N-terminal acetylation of proteins were treated as variable modifications. Rigorous identification criteria were implemented, ensuring that both protein and peptide-level false discovery rates (FDR) remained <1%, with peptide confidence established at 99%. The extracted ion chromatogram width was limited to a maximum of 75 ppm. Protein quantification was conducted using the MaxLFQ algorithm (9).

Proteomics statistical analyses. The proteomic data analysis was performed using the Majorbio Cloud Platform (version 3.0; https://cloud.majorbio.com), accessible at https://cloud.majorbio.com. To evaluate the differences in protein expression between the two experimental groups, the R software (version 4.3.1; R Foundation for Statistical Computing) and the 'statmod' package (version 1.5.0) (10). Protein fold changes (FC) and corresponding P-values were computed to identify differentially expressed proteins (DEPs). DEPs were defined by stringent criteria: FC >1.2 or <0.83 combined with a P-value <0.05, ensuring the reliable selection of proteins with statistically significant expression differences. To evaluate the consistency of biological replicates and the degree of proteomic similarity between samples, Pearson's correlation analysis was performed. The entire proteomic dataset was further subjected to functional annotation using authoritative databases, including Gene Ontology (GO; http://geneontology.org/) and the Kyoto Encyclopedia of Genes and Genomes (KEGG; http://www.genome.jp/kegg/). This annotation facilitated the interpretation of biological roles and pathways associated with the DEPs. Enrichment analyses of GO terms and KEGG pathways were subsequently performed to reveal the biological relevance of these proteins. Additionally, protein-protein interaction (PPI) networks were constructed employing the STRING database (version 11.5; https://string-db.org/; STRING Consortium) (11) to visualize the interactions among DEPs, thereby enhancing comprehension of their functional interplay within the examined biological system.

Metabolite extraction. A total of ~100 mg of solid tissue was transferred into a 2 ml microcentrifuge tube, followed by the addition of a 6 mm stainless steel grinding bead to facilitate homogenization. Metabolite extraction commenced upon adding 800 μl methanol-water solution (4:1, v/v) to each sample, supplemented with four internal standards, including L-2-chlorophenylalanine at a concentration of 0.02 mg/ml. The homogenization procedure was carried out utilizing a frozen tissue grinder (model Wonbio-96c; Shanghai Wonbio Biotechnology Co., Ltd.), with the temperature maintained at -10˚C and the operating frequency set at 50 Hz for a duration of 6 min. Following the initial homogenization, the resulting homogenates underwent ultrasonic-assisted extraction, which was performed at a controlled temperature of 5˚C and a frequency of 40 kHz for a period of 30 min. Once the extraction process was completed, the samples were left to incubate at -20˚C for 30 min. This was succeeded by centrifugation at a high speed of 13,000 x g for 15 min at 4˚C, ensuring the proper separation of the components within the samples for subsequent analysis. The supernatants obtained were gathered and placed into autosampler vials for further analysis using LC-MS/MS.

Quality control (QC) sample. To guarantee stability within the system and uphold the quality of analytical control, a pooled QC sample was created by amalgamating equal portions from each individual sample. The preparation and analysis processes for these QC samples were consistent with those applied to the experimental samples. Acting as a representative for the complete dataset, the pooled QC was injected at regular intervals-namely, following every six analytical runs-to evaluate and oversee instrument performance and signal stability during the LC-MS/MS analysis.

Ultra performance LC-tandem MS (UPLC-MS/MS) analysis. The samples were analyzed utilizing LC-MS/MS on a cutting-edge UHPLC-Orbitrap Exploris 240 system (Thermo Fisher Scientific, Inc.). This advanced system was equipped with an ACQUITY HSS T3 column (100 mm in length and has an internal diameter of 2.1 mm with a particle size of 1.8 μm; Waters Corporation), which measures 100 mm in length and has an internal diameter of 2.1 mm with a particle size of 1.8 μm, and was provided by Waters Corporation. The experiments were performed at Shanghai Majorbio Bio-Pharm Technology Co. Ltd., ensuring access to high-level analytical resources. To facilitate the chromatographic process, a mobile phase system was utilized, consisting of two primary solvents.

Solvent A was prepared by dissolving 0.1% formic acid in a water-acetonitrile mixture at a volumetric ratio 2:98, whereas Solvent B consisted of pure acetonitrile containing 0.1% formic acid. Chromatographic separation was conducted under tightly controlled conditions, maintaining a flow rate of 0.40 ml/min and a column temperature of 40˚C. For each analysis, 5 μl sample was injected to ensure precision and reproducibility.

The MS analysis employed a UHPLC system coupled to a UHPLC-Orbitrap Exploris 240 mass spectrometer equipped with an electrospray ionization source, capable of operating in both positive and negative ion modes. Instrument parameters were carefully optimized, with the source temperature set at 400˚C, sheath gas flow at 40 arbitrary units and auxiliary gas flow at 10 arbitrary units. The ion spray voltage floating was adjusted to -2,800 V in negative mode and 3,500 V in positive mode to promote efficient ionization of analytes. Fragmentation was facilitated using MS/MS with normalized collision energies of 20, 40 and 60 V applied via a rolling collision energy approach to enhance fragmentation efficiency and specificity. Data acquisition was performed using a data-dependent acquisition strategy, collecting mass spectra across an m/z range of 70 to 1,050. This comprehensive acquisition method ensured enhanced data quality and coverage, supporting thorough identification and characterization of compounds.

Metabolic data analysis. The initial processing of raw data derived from LC/MS was performed using Progenesis QI software (version 3.0; Waters Corporation). This sophisticated platform enabled the construction of a three-dimensional data matrix saved in CSV format, incorporating essential elements such as sample identifiers, metabolite names and corresponding mass spectral intensity values, all critical for subsequent analyses. Internal standard peaks and known contaminants including noise, column bleed and derivatization reagent signals were carefully removed to ensure data integrity. Following this refinement, data redundancy was minimized by pooling similar peaks. Metabolite identification was performed through comprehensive cross-referencing against multiple databases, primarily the Human Metabolome Database (HMDB, http://www.hmdb.ca/), the METLIN database (https://metlin.scripps.edu/) and the proprietary Majorbio Database (MIDB) maintained by Shanghai Majorbio Biotechnology Co., Ltd. This rigorous approach facilitated accurate and reliable metabolite profiling.

To ensure reliable compound annotation, metabolite identification followed explicit criteria based on the database-matching workflow. Specifically, precursor ions were required to meet a mass accuracy threshold of <10 ppm, and metabolite assignment further required a MS/MS spectral match score above the identification cutoff used in Progenesis QI. Precursor and fragment ions were matched against entries in HMDB, METLIN and the Majorbio in-house MIDB database to support putative metabolite identities.

The data matrix, which was annotated based on database searches, was subsequently uploaded to the Majorbio cloud platform (https://cloud.majorbio.com) for additional analysis. The preprocessing of this data matrix involved retaining metabolic features that were present in ≥80% of the samples from any experimental group. For the treatment of missing values, the minimum value observed within the dataset was used for substitution, and each metabolic feature underwent normalization relative to the overall signal sum. To address variability that could stem from inconsistencies in sample preparation and instrument fluctuations, mass spectrometric peak intensities were subjected to sum normalization, resulting in a normalized data matrix. Variables linked to QC samples showing a relative standard deviation >30% were removed, and the data was log10 transformed to stabilize the variance, culminating in the final matrix ready for subsequent analyses. Variance analysis was then performed on this refined dataset.

For the purpose of conducting multivariate statistical analyses, the R package 'ropls' (version 1.6.2; https://bioconductor.org/packages/ropls/) was employed to execute principal component analysis (PCA) alongside orthogonal partial least squares discriminant analysis (OPLS-DA). The model's robustness was assessed via a seven-cycle interactive cross-validation method. Metabolites were deemed statistically significant if they exhibited a variable importance in projection (VIP) score >1 within the OPLS-DA framework and a P-value <0.05, evaluated using an unpaired Student's t-test.

The metabolites demonstrating considerable differences between the two groups were comprehensively organized into different biochemical pathways by employing metabolic enrichment and pathway analysis, utilizing the information available from the KEGG database. This process involved categorizing the metabolites based on their corresponding biological functions or pathways. To assess whether certain functional groups of metabolites were statistically overrepresented, an enrichment analysis was performed. This approach allowed for a broader interpretation of the data, moving beyond the identification of single metabolites to a more holistic group-level understanding. The enrichment analysis was made possible through the utilization of the Python package 'scipy.stats' (https://docs.scipy.org/doc/scipy/), which served a crucial role in pinpointing the biological pathways that were most pertinent to the specific experimental conditions under study.

Statistical correction for multiple comparisons. For all metabolomic and proteomic comparisons, P-values were adjusted using the Benjamini Hochberg FDR procedure, as implemented on the Shanghai Majorbio Cloud Platform. Differential metabolites and proteins were considered significant only after FDR correction in addition to predefined fold-change or VIP thresholds.

Results

Each of the two groups, invasive and non-invasive, included 8 patients. The clinical and radiological characteristics of these cohorts are detailed in Table I. Patients in the invasive group were significantly older than those in the non-invasive group (59.3±11.1 vs. 55.4±8.1 years; P=0.0006). Regarding tumor morphology, the invasive group demonstrated a substantially larger median preoperative tumor volume [7,777.5 (5,398.9, 9,202.6) cm^3] compared with the non-invasive group [3,117.7 (1,570.7, 3,605.9) cm^3; P=0.0121]. Additionally, all 8 patients in the invasive cohort were classified as Knosp grade ≥2, whereas none of the patients in the non-invasive cohort met this threshold (P>0.9999). No significant difference was observed in the sex distribution between the two groups (P=0.6199).

Table I. Baseline characteristics of the patients with pituitary adenoma included in the study.

Characteristic	Invasive group (n=8)	Non-invasive group (n=8)	P-value[a]
Age, years	59.3 (11.1)	55.4 (8.1)	0.0006
Sex[b], n (%)			0.6199
Male	5 (62.5)	3 (37.5)	
Female	3 (37.5)	5 (62.5)	
Tumor volume[c], cm^3	7,777.5 (5,398.9, 9,202.6)	3,117.7 (1,570.7, 3,605.9)	0.0121
Invasive (Knosp grade ≥2), n (%)	8 (100)	0 (0)	>0.9999

Data are shown as the mean ± SD or median (25th percentile, 75th percentile). [a]Between-group comparisons were performed using an unpaired Student's t-test; [b]sex distribution was compared using Fisher's exact test; [c]preoperative tumor volume.

These results confirm significant baseline differences in tumor aggressiveness and volume between the two study groups (Table I).

Identification of DEPs. Quantitative proteomics analysis revealed 614 DEPs between the invasive and non-invasive groups. To gain insight into group-specific functional differences, unsupervised hierarchical clustering was performed on these proteins (Fig. 1). The results indicated low Pearson's correlation coefficients of protein expression among samples within groups, but high Pearson's correlation coefficients between groups, suggesting clear proteomic differences between the groups, whereas the proteomic profiles within each group were relatively stable.

Subsequent comparative analyses were conducted to identify and visualize DEPs between the invasive and non-invasive groups using volcano plots. In total, 286 proteins exhibited upregulation, while 328 proteins showed downregulation in the invasive group when compared with the non-invasive cohort (Fig. 2A). The most upregulated proteins in the invasive group included vesicle-associated membrane protein 2 (VAMP2) and T-cell lymphoma invasion and metastasis-inducing protein 1, while tubulin b1 class VI (TUBB1) was among the most significantly downregulated proteins (Fig. 2B-D).

Pathway enrichment analysis of DEPs. An analysis of enrichment was performed on the DEPs to assess their functional significance. The GO analysis indicated a notable enrichment of DEPs in various biological processes and components, including the 'regulation of gonadotropin secretion', 'gated channel activity' and their localization at the 'postsynaptic membrane' (Fig. 3A). Furthermore, a pathway analysis utilizing the KEGG suggested that these proteins were primarily associated with the 'cyclic adenosine monophosphate (cAMP) signaling pathway', 'cytokine-cytokine receptor interaction', as well as 'pancreatic secretion' (Fig. 3B).

Identification of differentially expressed metabolites (DEMs). A comparative study was performed to identify and illustrate the DEMs between the groups classified as invasive and non-invasive, utilizing a volcano plot for visualization. In the invasive group, 42 metabolites showed increased expression, while 32 metabolites were found to be decreased when compared with the non-invasive group (Fig. 4A). Compared with the non-invasive group, the metabolites that showed a significant increase in the invasive group included 3-hydroxyoctanoic acid, whereas L-glycine and Gpetn(18:3/22:4) exhibited a notable decrease (Fig. 4B-D).

Metabolomics enrichment analysis. The examination of KEGG pathway enrichment for the DEMs within the invasive and non-invasive groups revealed significant enrichment across multiple biological pathways. These pathways included the 'primary bile acid biosynthesis', 'protein digestion and absorption', 'alpha-linolenic acid metabolism', the 'cAMP signaling pathway', the 'synaptic vesicle cycle' and pathways associated with b 'pathogenic *Escherichia coli* (*E. coli*) infection' (Fig. 5).

Combined proteomics and metabolomics analyses. The results indicated that the proteins and metabolites that were expressed differently in the invasive and non-invasive groups were significantly enriched in pathways related to pathogenic *E. coli* infection, the synaptic vesicle cycle and cAMP signaling. This convergence suggests that these biological pathways may be critically involved in the mechanisms underlying pituitary tumor invasiveness (Fig. 6).

Discussion

The present study employed an integrative proteomic and metabolomic approach to elucidate the molecular mechanisms underlying the invasive phenotype of pituitary adenomas. By comparing IPAs with non-invasive adenomas, distinct molecular profiles were characterized at both protein and metabolite levels, identifying pathways potentially contributing to tumor invasiveness (12). The findings revealed unique proteomic and metabolic changes in invasive tumors, marked by differential expression of key proteins and metabolites enriched in three critical pathways: The cAMP signaling cascade, pathogenic *E. coli* infection and the synaptic vesicle cycle. These results offer new insights into the molecular mechanisms driving the aggressive behavior observed in a subset of pituitary adenomas.

cAMP, originally identified as the first second messenger, is critical in intracellular signaling pathways and regulates a broad spectrum of physiological and pathological processes (13). Its regulatory actions are chiefly mediated through activation of protein kinase A (PKA), which initiates downstream signaling

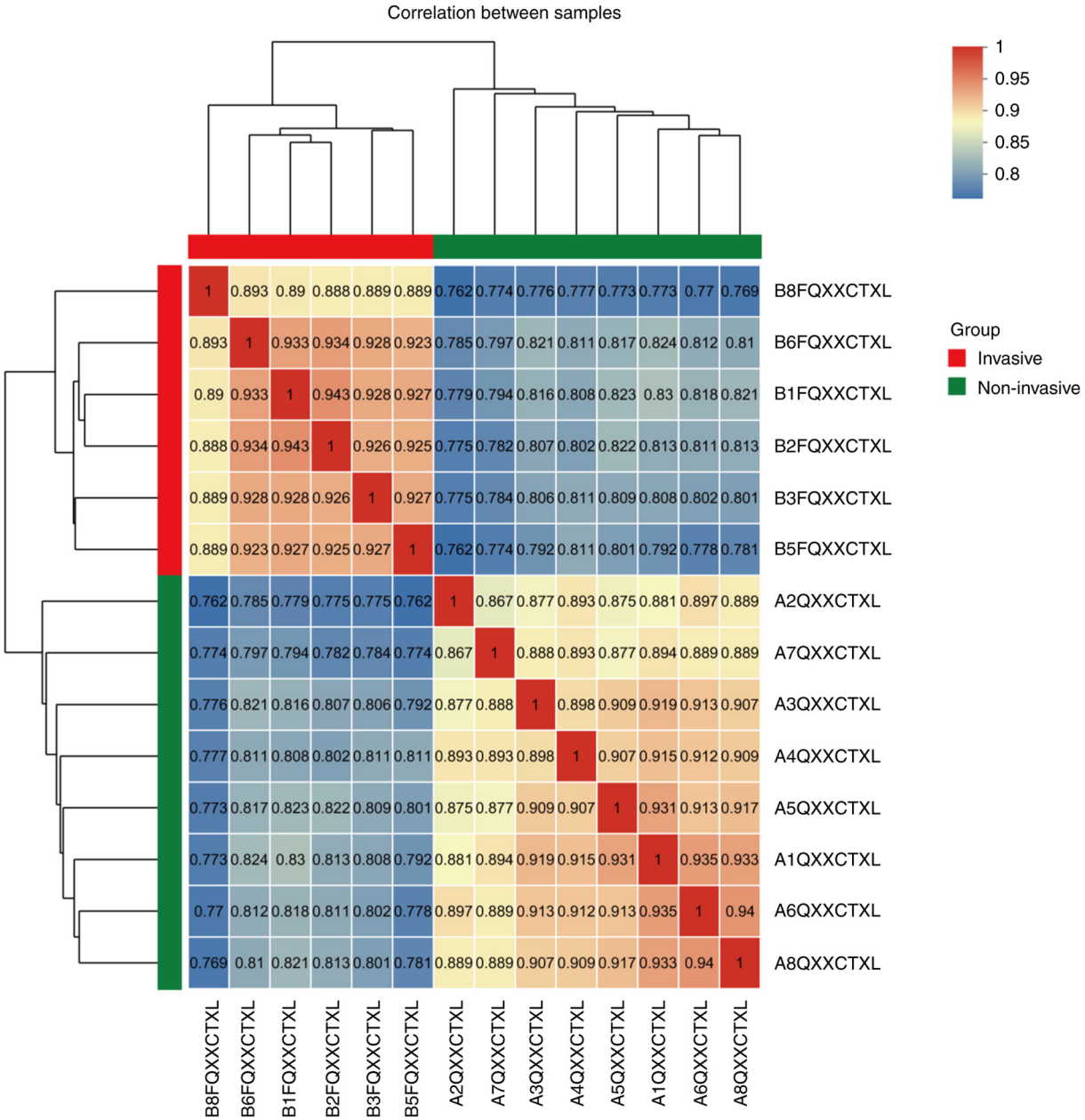

Figure 1. Correlation heat map of differential protein samples between the invasive group and non-invasive group.

events, including modulation of gene transcription via the cAMP response element-binding protein (14). Furthermore, PKA phosphorylates various kinases, such as Raf and glycogen synthase kinase 3 (15,16). Altered signaling of cAMP-PKA has been linked to various human tumors. Previous research has indicated that the cAMP signaling pathway serves a role in several types of cancer, with its tumor-promoting effects observed in hepatocellular carcinoma, lung cancer, ovarian cancer, colorectal cancer and melanoma (17-21). Moreover, as a classical signaling cascade, the cAMP pathway has been demonstrated to promote the progression of pituitary adenomas (22-24). The present data provide further evidence supporting the involvement of the cAMP pathway in the invasiveness of pituitary adenomas.

The KEGG pathway annotated as 'pathogenic *Escherichia coli* infection' emerged as enriched in IPAs; however, this does not imply the physical presence of bacteria within the tumor tissue. Instead, this KEGG category mainly reflects a set of host cellular processes that pathogenic *E. coli* manipulate during infection, particularly actin cytoskeleton remodeling, focal adhesion reorganization, membrane trafficking and junctional disruption (25,26). These same host-driven processes are well-recognized hallmarks of cancer cell invasion (27). Pathogenic *E. coli* effectors such as Tir, EspF and Map activate MAPK, Rho GTPases and NF-κB pathways to induce cytoskeletal rearrangement and promote pedestal formation in epithelial cells; however, these pathways are fundamentally host signaling modules that can be engaged in numerous non-infectious contexts, including tumor progression (28). Therefore, the enrichment of this pathway in invasive adenomas likely reflects activation of actin-modifying, adhesion-modulating and endocytosis-related host programs that overlap mechanistically with those annotated

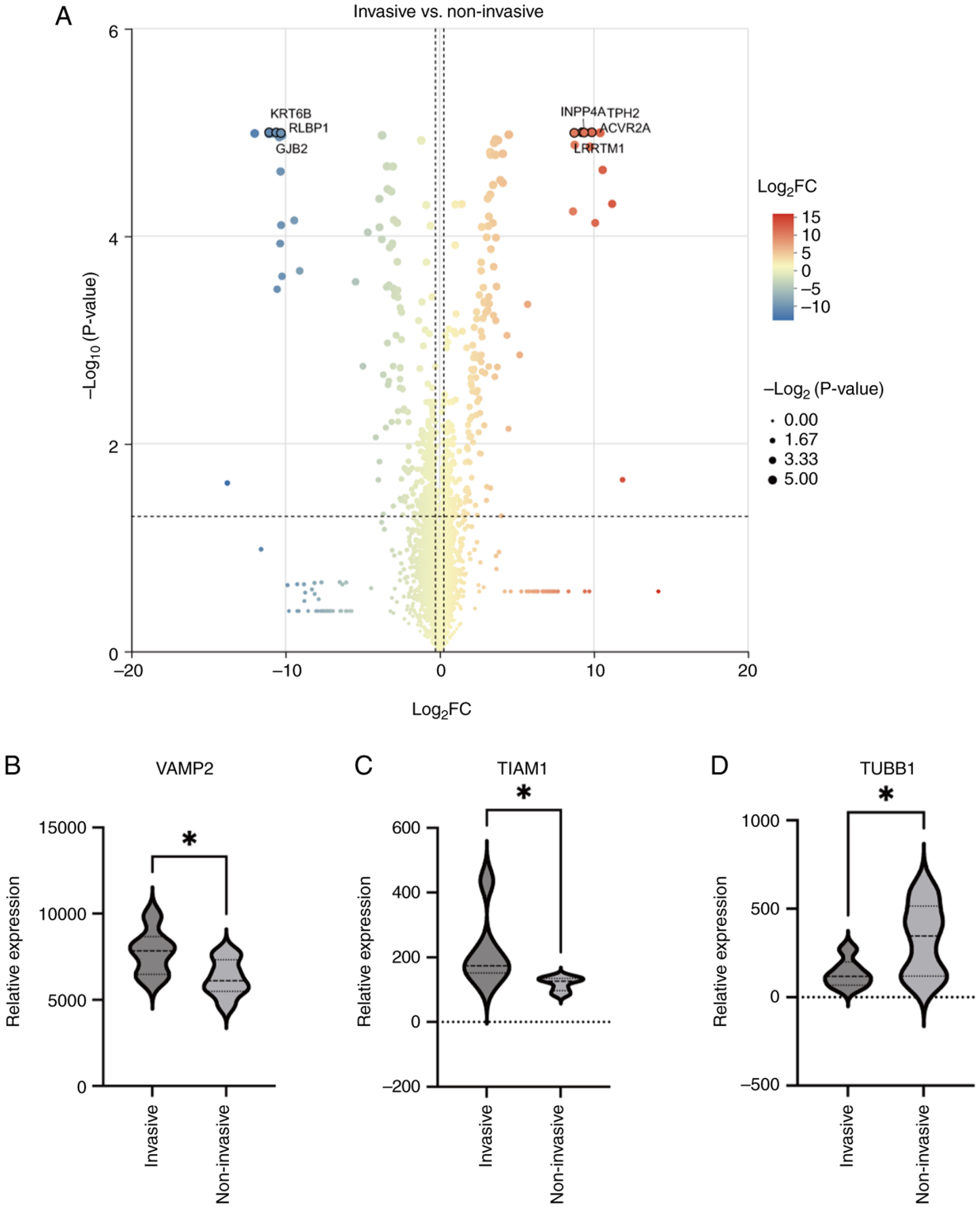

Figure 2. Statistics of differentially expressed proteins between the invasive group and the non-invasive group, and between the invasive group and the non-invasive group. (A) A Volcano plot of P-value vs. $\log_2$(FC) in the control group compared with the invasive group. Significantly upregulated and downregulated proteins are highlighted (FC >1.2; P≤0.05). Violin plot presenting differentially expressed proteins (B) VAMP2, (C) TIAM1 and (D) TUBB1 between the invasive group and the non-invasive groups. *P<0.05. FC, fold change.; VAMP2, vesicle-associated membrane protein 2; TIAM1, T-cell lymphoma invasion and metastasis-inducing protein 1; TUBB1, tubulin b1 class VI.

under bacterial infection (27). In this sense, the '*E. coli* infection' label represents a functional signature of cytoskeletal and membrane-dynamics pathways relevant to cellular motility and invasion, rather than evidence for microbial involvement.

However, beyond host signaling, the emerging role of the tumor microbiome must also considered. Although the pituitary gland has traditionally been viewed as a sterile environment, landmark studies have previously revealed the presence of intratumoral bacteria across various tumor types, suggesting a potential role in carcinogenesis and therapeutic response (29-31). In the specific context of pituitary adenomas, recent investigations have identified distinct alterations in the gut microbiota of patients with invasive tumors compared with those with non-invasive subtypes, implying a functional

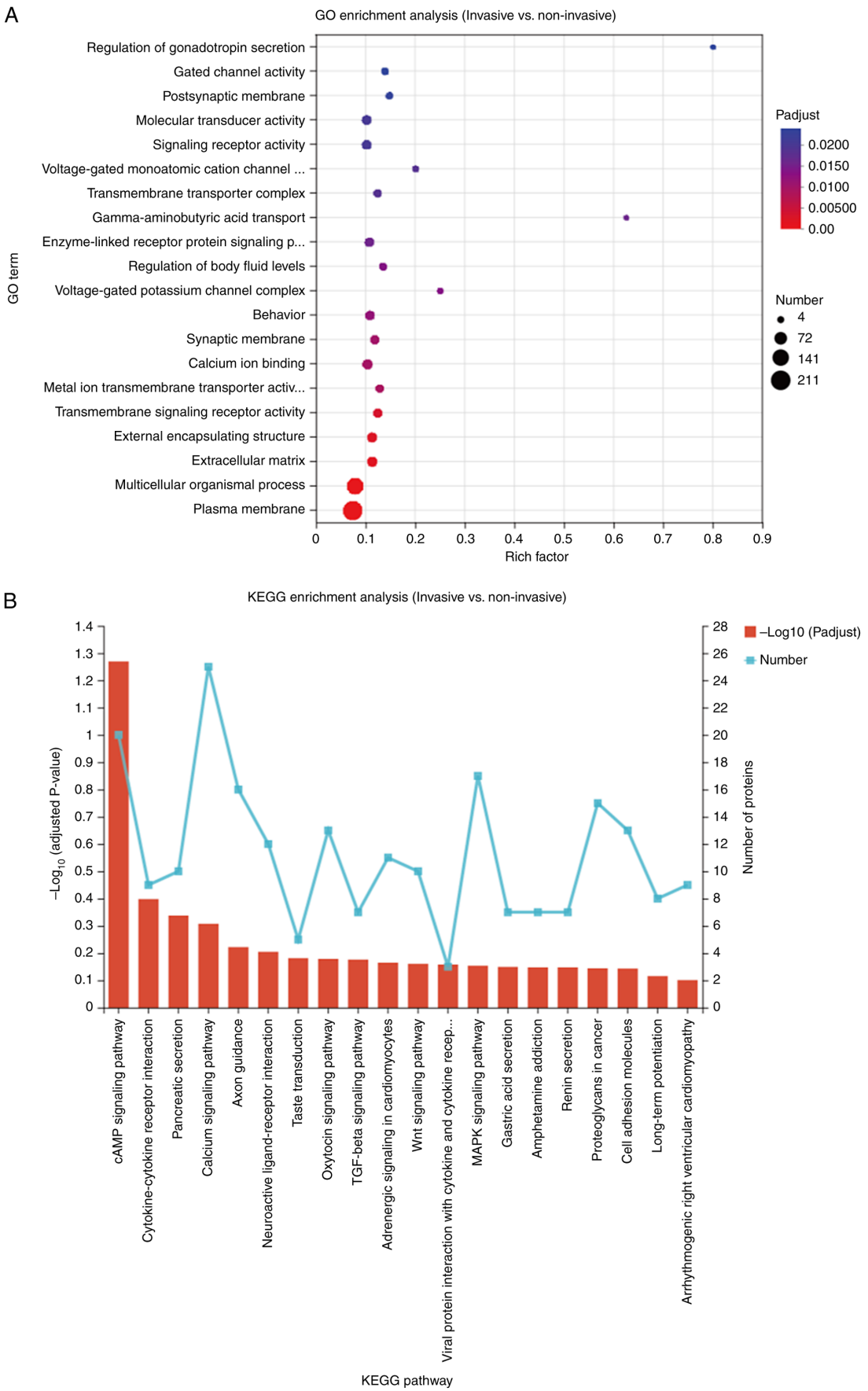

Figure 3. Functional enrichment analysis of DEPs between the invasive group and the non-invasive group. (A) The 20 GO terms that are most enriched, based on the DEPs, display significantly modified expression patterns (FC >1.2; FDR-adjusted P≤0.05). The X-axis displays the Rich factor, with the color of the dot reflecting the significance of the change in expression (adjusted P-value). The size of the dot represents the number of proteins linked to each GO term. (B) KEGG pathway analysis of differentially expressed genes. DEPs, differentially expressed proteins; FDR, false discovery rate; FC, fold change; GO, Gene Ontology; KEGG, Kyoto Encyclopedia of Genes and Genomes.

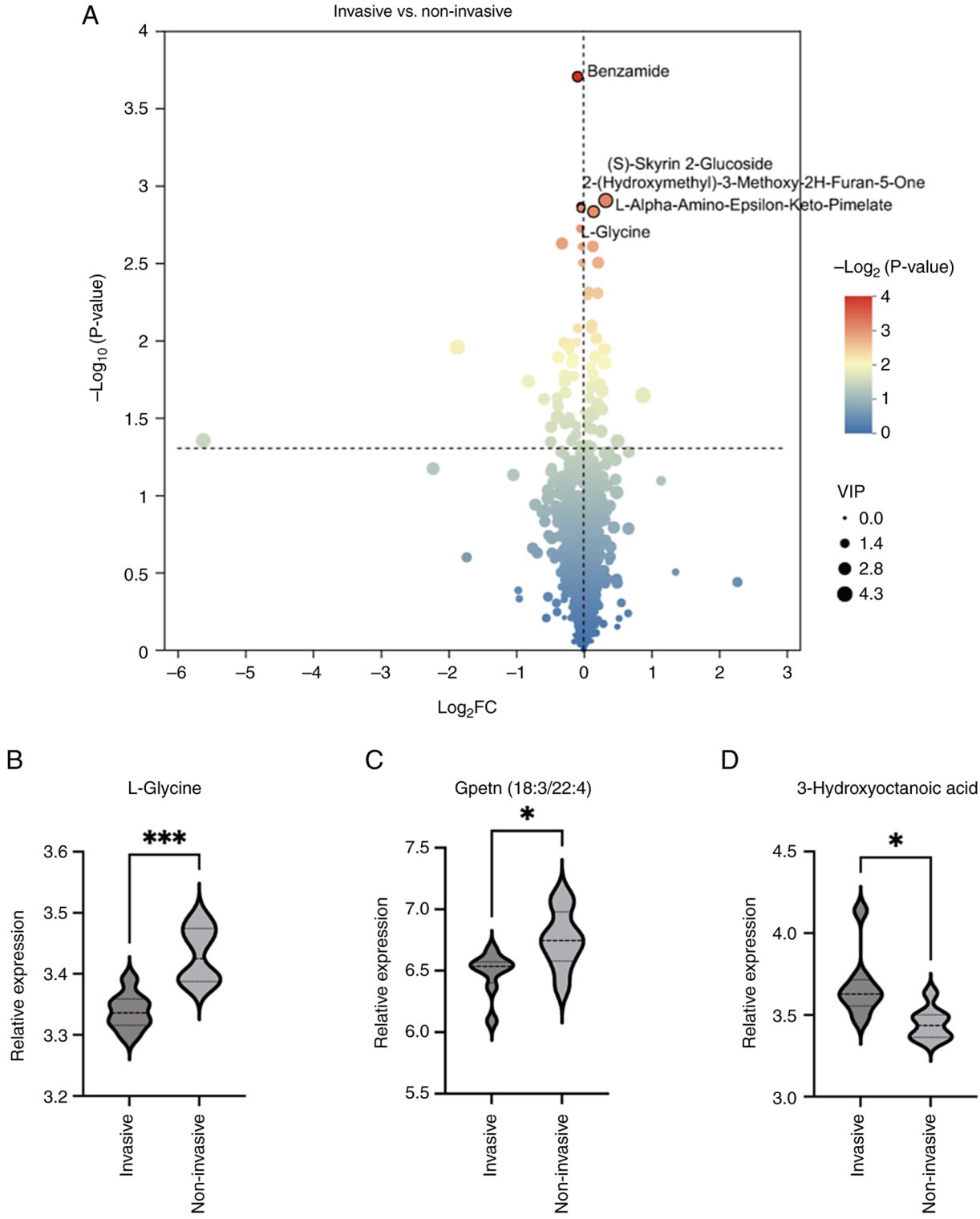

Figure 4. Identification and visualization of differential metabolites in invasive vs. non-invasive pituitary adenomas. (A) Overview of differential metabolites identified in the invasive group compared with the non-invasive group. Violin plots displaying metabolites (B) L-glycine, (C) Gpetn(18:3/22:4) and (D) 3-hydroxyoctanoic acid that showed differential expression across the invasive and non-invasive groups. *P<0.05 and ***P<0.001. FC, fold change.

'gut-pituitary axis' (32). Furthermore, theoretical frameworks suggest that microbial metabolites could influence pituitary tumor behavior and hormonal secretion through systemic circulation (33). While the present study focuses on host proteomic changes, the detection of infection-related pathways highlights the need to consider these potential microbial-host crosstalk mechanisms in future comprehensive studies.

The synaptic vesicle cycle refers to the tightly regulated process by which neurons release neurotransmitters at synapses and then recycle the vesicle components for repeated use (34). This cycle involves several key steps: Vesicle docking, priming, Ca^{2+}-dependent exocytosis, endocytosis and vesicle recycling (35). Essential proteins in this pathway include SNARE complexes, synaptotagmins, Rab GTPases and clathrin-mediated

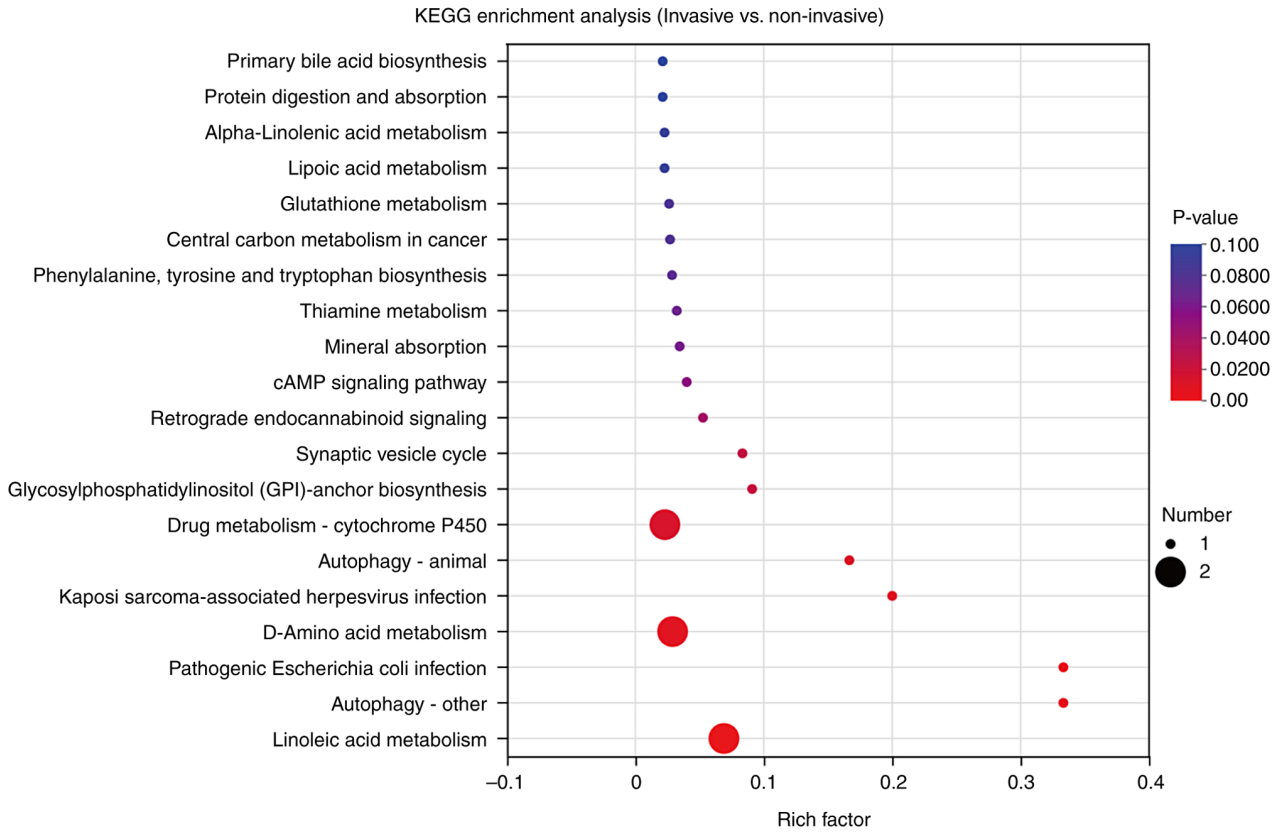

Figure 5. Functional enrichment analysis of differential metabolites between the invasive group and the non-invasive group.

endocytosis components. These proteins coordinate membrane fusion and retrieval, maintaining synaptic transmission fidelity and plasticity (36). Although traditionally studied in the nervous system, previous evidence suggests that components of the synaptic vesicle cycle are aberrantly expressed or repurposed in various cancers. For instance, proteins such as synaptotagmin have been found to be dysregulated in gliomas (37). In particular, previous studies have revealed that functional synaptic connections can form between neurons and malignant brain tumors, such as high-grade gliomas (38-40). By contrast, direct evidence for such synaptic-like interactions in pituitary adenomas is currently lacking. Therefore, while the upregulation of synaptic vesicle cycle components in IPAs is intriguing, any similarities to neuron-glioma interactions should be regarded strictly as hypothesis-generating rather than indicative of established tumor-neuron synaptic communication (41). In the present study, the significant enrichment of synaptic vesicle recycling pathways in IPAs suggests that elements of vesicle trafficking and membrane dynamics may be exploited to promote tumor invasiveness.

In the present study, IPAs displayed significant enrichment of synaptic vesicle cycling components. This observation raises an important mechanistic question: How might the cAMP-PKA pathway intersect with vesicle-trafficking regulation in tumor cells? In neurons, cAMP-activated PKA is a central modulator of presynaptic release. PKA phosphorylates synapsin I, promoting the mobilization of synaptic vesicles from the reserve pool to the readily releasable pool, thereby increasing vesicle availability for exocytosis (42). PKA also phosphorylates key SNARE-associated regulators such as tomosyn, reducing its inhibitory interaction with syntaxin-1 and facilitating SNARE-complex assembly (43) and snapin, whose phosphorylation strengthens the SNAP-25 interaction and enhances vesicle priming (44).

Although VAMP2 itself is not a direct PKA substrate, PKA-driven modulation of upstream regulators creates a biochemical environment that favors efficient assembly of VAMP2 with syntaxin-1 and SNAP-25, ultimately increasing vesicle fusion probability (45). This mechanistic framework is highly relevant to the proteomic findings. VAMP2, one of the most significantly upregulated proteins in invasive adenomas, is a v-SNARE essential for membrane fusion and has been implicated in promoting integrin trafficking and cancer cell migration. In non-neuronal cancer systems, VAMP2 mediates α5β1-integrin delivery to the plasma membrane, and its depletion reduces cell adhesion, motility and viability (46,47). Therefore, in a tumor context with heightened cAMP-PKA activity, increased phosphorylation of synapsin, tomosyn and snapin may enhance vesicle priming, accelerate SNARE-complex assembly and potentiate trafficking of pro-invasive cargos (such as integrins, metalloproteinases and growth factors) to the plasma membrane. Such coordinated enhancement of vesicle dynamics provides a biologically plausible rationale for the concurrent enrichment of cAMP signaling and the synaptic vesicle cycle in IPAs. Together, these data support a model in which invasive tumors co-opt neuro-modulatory exocytosis programs to facilitate membrane remodeling, microenvironmental interactions and ultimately invasion.

In addition to pathway-level alterations, several of the top-ranked DEPs and DEMs provide further insight into the invasive phenotype. Although VAMP2 has already been

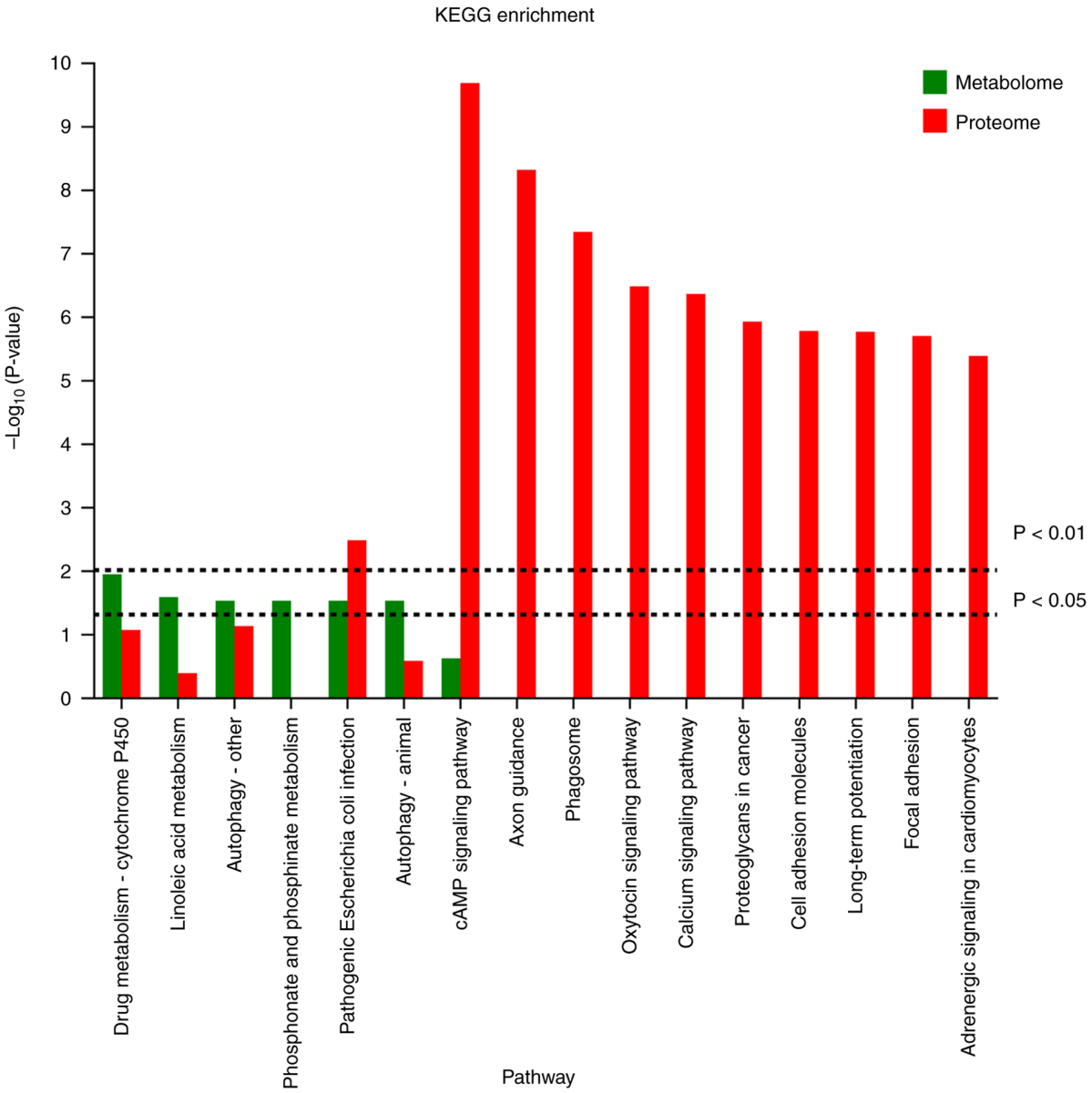

Figure 6. Combined analysis of differential proteins and metabolites between the invasive group and the non-invasive group. KEGG, Kyoto Encyclopedia of Genes and Genomes.

discussed in the context of vesicle trafficking, its upregulation in IPAs is consistent with prior evidence showing that VAMP2 facilitates integrin delivery, membrane fusion and motility in cancer cells (47), supporting its relevance to invasion. Conversely, the marked downregulation of TUBB1, a β-tubulin isoform involved in microtubule stability, aligns with previous studies demonstrating that altered tubulin composition can enhance cytoskeletal plasticity, chromosomal instability, and migratory capacity in malignant cells (48). On the metabolic side, the elevated level of 3-hydroxyoctanoic acid, a hydroxy fatty acid and endogenous agonist of HCA3, is notable because activation of this pathway has been linked to inflammatory signaling, metabolic rewiring and lipid utilization in tumor settings (49). Activation of the HCA3 pathway has been increasingly linked to inflammatory signaling, metabolic rewiring and lipid utilization within various tumor microenvironments. According to recent findings, 3-hydroxyoctanoic acid acts as a potent agonist that induces natural biased signaling at the HCA3 receptor (49). Unlike other structurally similar agonists, 3-hydroxyoctanoic acid leads to the notable recruitment of β-arrestin-2, a process that has been shown to be relevant for regulating cell-cell adhesion and altering spheroid density in 3D cell culture models. Specifically, the activation of HCA3 by 3-hydroxyoctanoic acid can result in less dense and larger cellular structures, suggesting that this metabolic signaling may weaken intercellular adhesion within the tumor mass. Furthermore, the HCA3-mediated signal involves Gβγ subunits and downstream effectors such as PI3K, Rac1 and Ras/Rho, which are crucial components for cellular motility and chemotaxis. In the context of IPAs, the accumulation of 3-hydroxyoctanoic acid may therefore prime tumor cells for a more infiltrative phenotype by facilitating microtubule remodeling and vesicle-mediated secretion (49). While traditionally viewed as an anti-inflammatory mediator, the HCA3 axis in pituitary adenomas likely coordinates metabolic adaptation to support the energetic demands of tumor invasion into adjacent structures such as the cavernous sinus. Together,

these molecular signatures suggest that IPAs may coordinate vesicle-mediated secretion, microtubule remodeling and fatty acid-driven metabolic adaptation to support a more motile and infiltrative phenotype.

From a clinical perspective, these molecular alterations offer potential biomarkers for the prediction of tumor invasiveness and may inform therapeutic strategies. For example, the cAMP analogue Tacladesine can inhibit the growth of lung cancer, colon cancer, breast cancer, fibrosarcoma and leukemia *in vitro* and *in vivo* (50). Moreover, the integration of proteomic and metabolomic data enhances the ability to map functional networks, offering a more comprehensive view of tumor biology than either approach alone.

However, the present study has several limitations. A limitation is the relatively small sample size, which might reduce the statistical power required to detect minor differences and restrict the applicability of the results. Additionally, although the omics-focused analyses reveal connections between molecular alterations and invasiveness, they do not confirm a causal relationship. Functional validation of candidate proteins and metabolites is needed to confirm their mechanistic roles in tumor invasion. Finally, the heterogeneity of pituitary adenoma subtypes (such as hormonally active vs. inactive) was not stratified in the current analysis, which may confound some of the observed molecular patterns.

Future studies should expand the cohort size and include longitudinal data to assess whether these molecular markers are associated with treatment response or recurrence. Moreover, both *in vivo* and *in vitro* studies are necessary to assess the importance of crucial pathways, including cAMP signaling and synaptic vesicle cycling, in facilitating tumor invasiveness. Single-cell multi-omics approaches may further uncover cell-type-specific drivers of invasion and help to delineate tumor-microenvironment interactions. Finally, a specific limitation of the present study is the lack of metagenomic or 16S rRNA sequencing analysis. Since the present workflow was designed for host proteomics and metabolomics, we could not directly assess the microbiome composition. Therefore, although the enrichment of infection-related pathways was interpreted primarily as host cytoskeletal mimicry, the potential influence of the intratumoral or gut microbiome cannot be definitively ruled out. Future research should incorporate microbiome-specific approaches to explore whether direct bacterial-tumor interactions contribute to the invasive phenotype of pituitary adenomas.

In summary, the present integrative analysis highlights several signaling and metabolic pathways that may contribute to the invasive phenotype of pituitary adenomas. These findings advance the understanding of pituitary tumor biology and open new avenues for prognostic biomarker development and therapeutic intervention

Acknowledgements

Not applicable.

Funding

The present work was supported by the Natural Science Foundation of Fujian Province (grant nos. 2022J05315, 2023J011625, 2023J011622 and 2024J08322), the Medical Project of Xiamen Municipal Bureau of Science and Technology (grant no. 3502Z2024ZD1007), Xiamen Health High Quality Development Technology Plan Project (grant nos. 2024GZL-GG95 and 2024GZL-CX38), Medical and Health Guidance Program of Xiamen City, China (grant no. 3502Z20224ZD1012) and the Scientific Research Initiation Fund for Introduced Talents of the First Affiliated Hospital of Xiamen University (grant no. XYJ2023001).

Availability of data and materials

The proteomics data generated in the present study may be found in the iProX Consortium via the ProteomeXchange partner repository under the accession number PXD071754 or at the following URL: https://proteomecentral.proteomexchange.org/cgi/GetDataset?ID=PXD071754. The metabolomics data generated in the present study may be found in the MetaboLights repository under the accession number MTBLS13478 or at the following URL: https://www.omicsdi.org/dataset/metabolights_dataset/MTBLS13478.

Authors' contributions

JM, XC and JS designed the study and oversaw the implementation of the project. WZ and CW were responsible for the acquisition of clinical samples. BL, SC and GT carried out the data processing and interpreted the proteomic and metabolomic findings. JM, XC, WZ and BL wrote the original draft. BL, CW and JS reviewed and edited the manuscript. XC, PZ and JS were involved with conceptualization of the study. ZL and YL were responsible for the management of the proteomic and metabolomic databases and performed the formal statistical analysis. SC and GT performed project administration. JM, XC, WZ, ZL, CW and JL contributed to funding acquisition. JM and JS confirm the authenticity of all the raw data. All authors read and approved the final version of the manuscript.

Ethics approval and consent to participate

Approval of the research protocol by an Institutional Reviewer Board. The present study was reviewed and approved by the Ethics Committee of The First Affiliated Hospital of Xiamen University [approval no. 2023KYEC (070)]. The present study was performed in accordance with the principles of the Declaration of Helsinki and written informed consent about the participation in the research work was obtained from all patients before surgery.

Patient consent for publication

Not applicable.

Competing interests

The authors declare that they have no competing interests.

References

1. Molitch ME: Diagnosis and treatment of pituitary adenomas: A review. JAMA 317: 516-524, 2017.

2. Lefevre E, Chasseloup F, Hage M, Chanson P, Buchfelder M and Kamenický P: Clinical and therapeutic implications of cavernous sinus invasion in pituitary adenomas. Endocrine 85: 1058-1065, 2024.
3. Lu L, Wan X, Xu Y, Chen J, Shu K and Lei T: Prognostic factors for recurrence in pituitary adenomas: Recent progress and future directions. Diagnostics (Basel) 12: 977, 2022.
4. Chen L, White WL, Spetzler RF and Xu B: A prospective study of nonfunctioning pituitary adenomas: Presentation, management, and clinical outcome. J Neurooncol 102: 129-138, 2011.
5. Raverot G, Ilie MD, Lasolle H, Amodru V, Trouillas J, Castinetti F and Brue T: Aggressive pituitary tumours and pituitary carcinomas. Nat Rev Endocrinol 17: 671-684, 2021.
6. James EL and Parkinson EK: Serum metabolomics in animal models and human disease. Curr Opin Clin Nutr Metabolic Care 18: 478-483, 2015.
7. Kwon YW, Jo HS, Bae S, Seo Y, Song P, Song M and Yoon JH: Application of proteomics in cancer: Recent trends and approaches for biomarkers discovery. Front Med 8: 747333, 2021.
8. Knosp E, Steiner E, Kitz K and Matula C: Pituitary adenomas with invasion of the cavernous sinus space: A magnetic resonance imaging classification compared with surgical findings. Neurosurgery 33: 610-617, 1993.
9. Cox J, Hein MY, Luber CA, Paron I, Nagaraj N and Mann M: Accurate proteome-wide label-free quantification by delayed normalization and maximal peptide ratio extraction, termed MaxLFQ. Mol Cell Proteomics 13: 2513-2526, 2014.
10. Smyth GK: Linear models and empirical bayes methods for assessing differential expression in microarray experiments. Stat Appl Genet Mol Biol 3: 1-25, 2004.
11. Szklarczyk D, Kirsch R, Koutrouli M, Nastou K, Mehryary F, Hachilif R, Gable AL, Fang T, Doncheva NT, Pyysalo S, *et al*: The STRING database in 2023: Protein-protein association networks and functional enrichment analyses for any sequenced genome of interest. Nucleic Acids Res 51: D638-D646, 2023.
12. Casado-Vela J, Cebrián A, del Pulgar MT and Lacal JC: Approaches for the study of cancer: Towards the integration of genomics, proteomics and metabolomics. Clin Transl Oncol 13: 617-628, 2011.
13. Sassone-Corsi P: The cyclic AMP pathway. Cold Spring Harb Perspect Biol 4: a011148, 2012.
14. Steven A, Friedrich M, Jank P, Heimer N, Budczies J, Denkert C and Seliger B: What turns CREB on? And off? And why does it matter? Cell Mol Life Sci 77: 4049-4067, 2020.
15. Häfner S, Adler HS, Mischak H, Janosch P, Heidecker G, Wolfman A, Pippig S, Lohse M, Ueffing M and Kolch W: Mechanism of inhibition of raf-1 by protein kinase a. Mo Cell Biol 14: 6696-6703, 1994.
16. Jensen J, Brennesvik EO, Lai YC and Shepherd PR: GSK-3beta regulation in skeletal muscles by adrenaline and insulin: Evidence that PKA and PKB regulate different pools of GSK-3. Cell Signal 19: 204-210, 2007.
17. Wang M, Li Y, Wang R, Wang Z, Chen K, Zhou B, Zhou Z and Sun X: PKA RIα/a-kinase anchoring proteins 10 signaling pathway and the prognosis of colorectal cancer. J Gastroenterol Hepatol 30: 496-503, 2015.
18. Finger EC, Castellini L, Rankin EB, Vilalta M, Krieg AJ, Jiang D, Banh A, Zundel W, Powell MB and Giaccia AJ: Hypoxic induction of AKAP12 variant 2 shifts PKA-mediated protein phosphorylation to enhance migration and metastasis of melanoma cells. Proc Natl Acad Sci USA 112: 4441-4446, 2015.
19. Shaikh D, Zhou Q, Chen T, Ibe JCF, Raj JU and Zhou G: cAMP-dependent protein kinase is essential for hypoxia-mediated epithelial-mesenchymal transition, migration, and invasion in lung cancer cells. Cell Signal 24: 2396-2406, 2012.
20. Tonucci FM, Almada E, Borini-Etichetti C, Pariani A, Hidalgo F, Rico MJ, Girardini J, Favre C, Goldenring JR, Menacho-Marquez M and Larocca MC: Identification of a CIP4 PKA phosphorylation site involved in the regulation of cancer cell invasiveness and metastasis. Cancer Lett 461: 65-77, 2019.
21. McKenzie AJ, Campbell SL and Howe AK: Protein kinase A activity and anchoring are required for ovarian cancer cell migration and invasion. PLoS One 6: e26552, 2011.
22. Bizzi MF, Bolger GB, Korbonits M and Ribeiro-Oliveira Jr: Phosphodiesterases and cAMP pathway in pituitary diseases. Front Endocrinol (Lausanne) 10: 141, 2019.
23. Lania A, Mantovani G and Spada A: cAMP pathway and pituitary tumorigenesis. Ann Endocrinol (Paris) 73: 73-75, 2012,
24. Pertuit M, Barlier A, Enjalbert A and Gérard C: Signalling pathway alterations in pituitary adenomas: Involvement of gsα, cAMP and mitogen-activated protein kinases. J Neuroendocrinol 21: 869-877, 2009.
25. Singh AP, Sharma S, Pagarware K, Siraji RA, Ansari I, Mandal A, Walling P and Aijaz S: Enteropathogenic E. coli effectors EspF and Map independently disrupt tight junctions through distinct mechanisms involving transcriptional and post-transcriptional regulation. Sci Rep 8: 3719, 2018.
26. Croxen MA and Finlay BB: Molecular mechanisms of escherichia coli pathogenicity. Nat Rev Microbiol 8: 26-38, 2010.
27. Li X and Wang J: Mechanical tumor microenvironment and transduction: Cytoskeleton mediates cancer cell invasion and metastasis. Int J Biol Sci 16: 2014-2028, 2020.
28. Aseervatham J: Cytoskeletal remodeling in cancer. Biology (Basel) 9: 385, 2020.
29. Nejman D, Livyatan I, Fuks G, Gavert N, Zwang Y, Geller LT, Rotter-Maskowitz A, Weiser R, Mallel G, Gigi E, *et al*: The human tumor microbiome is composed of tumor type-specific intracellular bacteria. Science 368: 973-980, 2020.
30. Niño JL, Wu H, LaCourse KD, Kempchinsky AG, Baryiames A, Barber B, Futran N, Houlton J, Sather C, Sicinska E, *et al*: Effect of the intratumoral microbiota on spatial and cellular heterogeneity in cancer. Nature 611: 810-817, 2022.
31. Kalaora S, Nagler A, Nejman D, Alon M, Barbolin C, Barnea E, Ketelaars SLC, Cheng K, Vervier K, Shental N, *et al*: Identification of bacteria-derived HLA-bound peptides in melanoma. Nature 592: 138-143, 2021.
32. Hu J, Yang J, Chen L, Meng X, Zhang X, Li W, Li Z and Huang G: Alterations of the gut microbiome in patients with pituitary adenoma. Pathol Oncol Res 28: 1610402, 2022.
33. Nie D, Li C and Zhang Y: PitNETs and the gut microbiota: Potential connections, future directions. Front Endocrinol (Lausanne) 14: 1255911, 2023.
34. Südhof TC: The synaptic vesicle cycle. Ann Rev Neurosci 27: 509-547, 2004.
35. Chanaday NL, Cousin MA, Milosevic I, Watanabe S and Morgan JR: The synaptic vesicle cycle revisited: New insights into the modes and mechanisms. J Neurosci 39: 8209-8216, 2019.
36. Rizo J and Südhof TC: The membrane fusion enigma: SNAREs, Sec1/Munc18 proteins, and their accomplices-guilty as charged? Annu Rev Cell Dev Biol 28: 279-308, 2012.
37. Sheng B, Jiang Y, Wu D, Lai N, Ye Z, Zhang B, Fang X and Xu S: RNAi-mediated SYT14 knockdown inhibits the growth of human glioma cell line U87MG. Brain Res Bull 140: 60-64, 2018.
38. Taylor KR, Barron T, Hui A, Spitzer A, Yalçin B, Ivec AE, Geraghty AC, Hartmann GG, Arzt M, Gillespie SM, *et al*: Glioma synapses recruit mechanisms of adaptive plasticity. Nature 623: 366-374, 2023.
39. Venkatesh HS, Morishita W, Geraghty AC, Silverbush D, Gillespie SM, Arzt M, Tam LT, Espenel C, Ponnuswami A, Ni L, *et al*: Electrical and synaptic integration of glioma into neural circuits. Nature 573: 539-545, 2019.
40. Venkataramani V, Tanev DI, Strahle C, Studier-Fischer A, Fankhauser L, Kessler T, Körber C, Kardorff M, Ratliff M, Xie R, *et al*: Glutamatergic synaptic input to glioma cells drives brain tumour progression. Nature 573: 532-538, 2019.
41. Winkler F, Venkatesh HS, Amit M, Batchelor T, Demir IE, Deneen B, Gutmann DH, Hervey-Jumper S, Kuner T, Mabbott D, *et al*: Cancer neuroscience: State of the field, emerging directions. Cell 186: 1689-1707, 2023.
42. Greengard P, Valtorta F, Czernik AJ and Benfenati F: Synaptic vesicle phosphoproteins and regulation of synaptic function. Science 259: 780-785, 1993.
43. Baba T, Sakisaka T, Mochida S and Takai Y: PKA-catalyzed phosphorylation of tomosyn and its implication in Ca2+-dependent exocytosis of neurotransmitter. J Cell Biol 170: 1113-1125, 2005.
44. Chheda MG, Ashery U, Thakur P, Rettig J and Sheng ZH: Phosphorylation of Snapin by PKA modulates its interaction with the SNARE complex. Nat Cell Biol 3: 331-338, 2001.
45. Clementi F, Fesce R, Meldolesi J, Valtorta F, Hilfiker S, Pieribone VA, Czernik AJ, Kao HT, Augustine GJ and Greengard P: Synapsins as regulators of neurotransmitter release. Philosophical Transactions of the Royal Society of London Series B: Biological Sciences 354: 269-279, 1999.
46. Raja SA, Abbas S, Shah STA, Tariq A, Bibi N, Yousuf A, Khawaja A, Nawaz M, Mehmood A, Khan MJ and Hussain A: Increased expression levels of Syntaxin 1A and Synaptobrevin 2/vesicle-associated membrane protein-2 are associated with the progression of bladder cancer. Genet Mol Biol 42: 40-47, 2019.

47. Hasan N and Hu C: Vesicle-associated membrane protein 2 mediates trafficking of alpha5beta1 integrin to the plasma membrane. Exp Cell Res 316: 12-23, 2010.
48. Trisciuoglio D and Degrassi F: The tubulin code and tubulin-modifying enzymes in autophagy and cancer. Cancers (Basel) 14: 6, 2021.
49. Peters A, Rabe P, Krumbholz P, Kalwa H, Kraft R, Schöneberg T and Stäubert C: Natural biased signaling of hydroxycarboxylic acid receptor 3 and G protein-coupled receptor 84. Cell Commun Signal 18: 31, 2020.
50. Cho-Chung YS and Nesterova MV: Tumor reversion: Protein kinase A isozyme switching. Ann N Y Acad Sci 1058: 76-86, 2005.